ACOUSTIC FULL WAVEFORM TOMOGRAPHY OF MARINE REFLECTION SEISMIC DATA

A. Przebindowska, A. Kurzmann, D. Köhn, T. Bohlen

email: *anna.przebindowska@kit.edu*

keywords: *waveform tomography, marine seismic data*

ABSTRACT

Full waveform tomography (FWT) is an efficient inversion technique that exploits the full information content of the seismic data. Synthetic studies show the great resolution potential of the method, nevertheless application to field data is not a common standard yet. This study discusses some of the problems related with the inversion of marine data in the acoustic approximation. The application of waveform tomography to field data is an extremely nonlinear problem. The lack of low frequency information makes the waveform tomography strongly depending on the initial model. Moreover, elastic effects, attenuation, noise present in the data, as well as an unknown source signature will additionally reduce the performance of the inversion algorithm. To mitigate some of these problems it is necessary to preprocess the data, estimate an accurate starting model and source wavelet. To enable the convergence and to eliminate some of the artifacts, it is essential to apply various preconditioning methods, and to include any available a priori information on the model parameters, including the density information.

INTRODUCTION

The overall goal of marine exploration geophysics is to image geological structures. Among other methods, the full waveform tomography (FWT) proved to be an efficient tool for determining high-resolution multi-parameter models (P-wave velocity, S-wave velocity, density) of complex subsurface structures. In contrast to the traveltime tomography, waveform tomography utilizes the full information content of the observed seismograms, i.e. amplitudes and phases. Thus it has a potential to image structures that are smaller than the seismic wavelength. Advances in parallel computing technology, numerical methods, and the improving quality of seismic data make the application of FWT feasible today.

The objective of FWT is to find a model of the subsurface that explains the observed data. For that purpose the algorithm has to minimize the residuals between modeled and observed data in an iterative process. To solve this problem we need to generate synthetic data from a starting model (the forward problem) and apply an efficient method for minimizing the data misfit function. Our strategy is based on the adjoint method. The forward problem and backpropagation of the residual wavefield are solved using a parallel time domain finite difference code, (Bohlen, 2002). The forward modeling code applies perfectly matched layers to suppress artificial reflections from the model boundaries. The waveform inversion scheme is based on the general approach of Tarantola (1986a) and Mora (1987) formulated in the space-time domain. The inversion problem can be addressed in an elastic or acoustic manner by utilizing the elastic or acoustic wave equation, respectively. The elastic FWT is more complicated than the acoustic approach, because it has to simultaneously optimize three coupled elastic parameters and, as a result, it requires more computational power.

It is a common practice to apply the acoustic approach for seismic data from marine exploration, i. e. to streamer or to OBC data, as it leads to a significant reduction in computational cost. However, the elastic simulation would provide a better match to the acquired marine data, since they contain many elastic signals

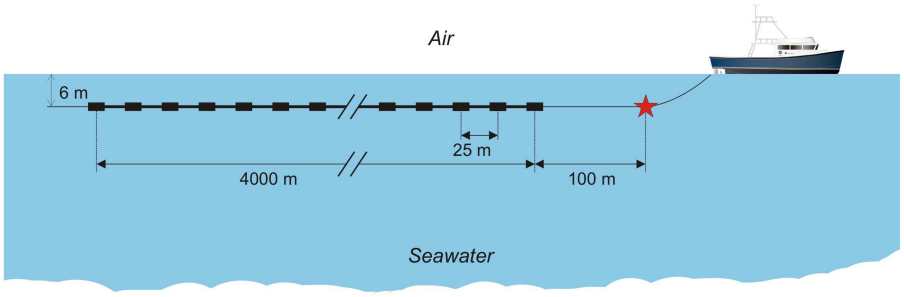

Figure 1: The acquisition geometry of the 2D marine data consists of a 160-channel, 4000 m streamer towed at the depth of 6 m. The source is an airgun array, a total amount of 1064 shots with a spacing of 25 m were recorded. The recorded trace length was 7 s with a sampling rate of 2 ms.

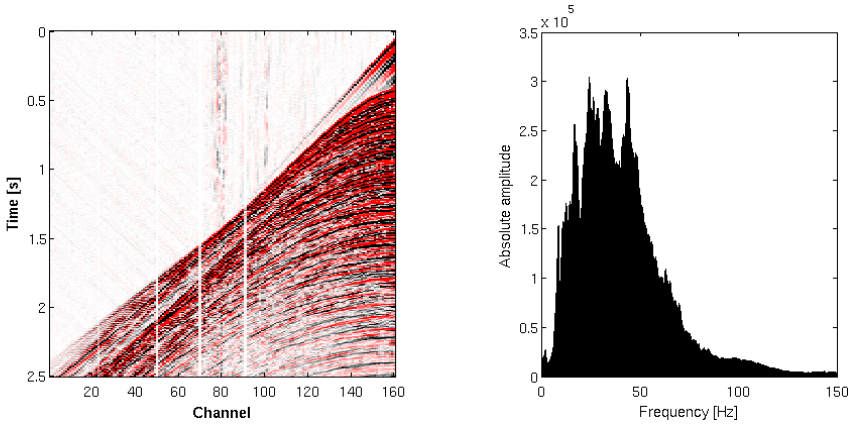

(a) **(b)**

Figure 2: (a) The representative common shot gather from the survey, with the corresponding amplitude spectrum (b). The vertical stripes in the data represent swell noise that has large amplitudes at relative low frequencies.

such as surface waves and mode converted waves. Nevertheless, it has been shown that the result of the acoustic inversion is reasonable when using marine seismic data. The elastic effects and anisotropy might limit the use of acoustic approach when considering the far offsets (Vigh, 2010).

This study presents the work in progress on the inversion of real data and discusses the problems that concern the field data preprocessing, generation of the starting model, wavelet estimation and the choice of different inversion strategies.

FIELD DATA PREPARATION

We apply the acoustic inversion to seismic data acquired in the North Sea. The survey gathered over 30 km of 2D seismic data. There are sonic logs available from four experimental well bores, located on the seismic line. They can be used to validate inversion results. From the available data, we selected a sub-region that extends over 3.1 km and consists of 50 shots (shot spacing 50 m). This relatively small portion of the data is used for test purposes, in order to reduce the computation time.

Prior to the inversion of the velocity structures, a specific preprocessing has to be applied to the raw field data. This data preparation is a fundamental step for FWT. Main objectives are to fit observed and synthetic seismograms, to improve S/N ratio, and to reduce the non-linearity of the inversion.

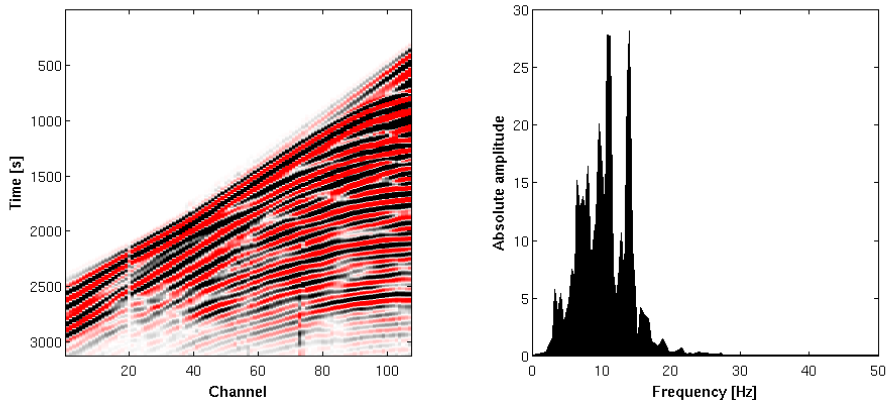

(a) (b)

Figure 3: (a) Observed data after preprocessing. The following steps have been applied: quality control (bad and noisy traces are edited); first arrival mute; time windowing to eliminate late arrivals; band-pass frequency filtering to remove low and high frequency noise; offset windowing; time resampling to satisfy the finite difference modeling stability conditions; 3D to 2D transformation

Frequency filtering/noise attenuation

A noise component is always present in seismic data. An efficient removal and/or attenuation of different noise types can be a challenging process, however it is a substantial issue in the waveform tomography. Marine noise comprises mainly noise generated due to hydrostatic pressure fluctuations, swell noise, noise from the vessel, and seismic interference, (Elboth et al., 2009). Hydrostatic pressure variations, i. e. changes of the water column height over the streamer, are caused by water swells and streamer buckling. The frequency content of this noise is limited up to 1-2 Hz. Another type of a high amplitude seismic noise in the marine environment is swell noise. This noise has large amplitudes at relatively low frequencies 2-10 (15) Hz and it usually affects a number of neighboring traces. Swell noise can be observed as vertical stripes in seismic data, Figure 2. Swell noise originates from the sea-surface waves and vibrations in the streamer caused by turbulent water related to these surface waves. On streamer operating during bad weather conditions, the hydrostatic pressure variations and swell noise are so strong that the signals from the data cannot be identified.

Low frequencies dominated by the hydrostatic pressure variations and swell noise can be removed by applying a low-cut filter, but it would also remove a large part of the seismic signal. Since low frequency data are crucial in the waveform tomography, we cannot apply a filter that eliminates or attenuates most of the unwanted noise while removing useful data. On the other hand without attenuating these high-amplitude noises the final inverted model would provide wrong information on the subsurface properties. Therefore, it would be necessary to implement a noise subtraction algorithm that mutes noise and preserves the useful signal at the same time.

3D to 2D transformation

The field data represent the wave propagation in a 3D medium, whereas the waveform modeling and inversion are implemented in 2D. This leads to a difference in the energy density and geometrical spreading between the field and synthetic data. In a homogeneous medium the energy for a 2D wave is not spread over the surface of a sphere (as in 3D case) but along the perimeter of a circle. The difference in the geometrical spreading between the 2D and 3D is significant and increases with the distance from the source. Moreover, in the 2D modeling an explosive source acts not as a point source but as a line source. This difference in the nature of the source that can be implemented in the 2D finite difference code results in changes of phase and amplitude of the data.

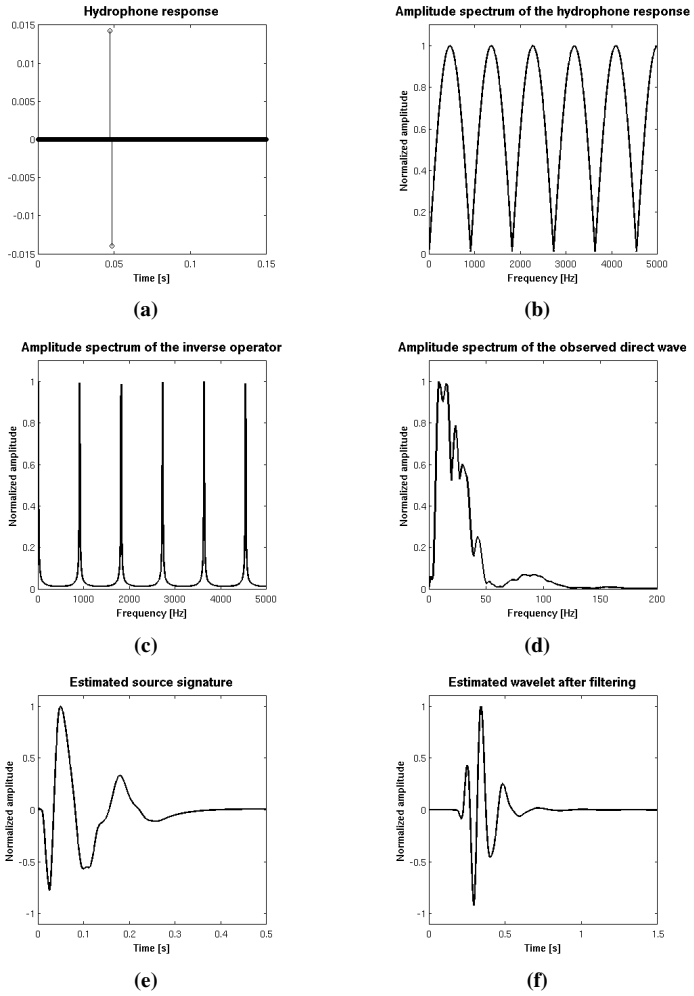

Figure 4: (a) Hydrophone group response to a horizontally traveling impulse, (b) with the corresponding amplitude spectrum. (c) Amplitude spectrum of the inverse of hydrophone response, (d) amplitude spectrum of the observed direct arrival waveform. (e) Estimated source wavelet with a bubble pulse obtained by convolving the direct arrival waveform with the inverse filter, (f) wavelet after filtering with Butterworth filter 3-14 Hz.

It is clear that with these approximations the modeled wavefield cannot be directly compared with the real data. Therefore, it is necessary to transform the field seismograms so that they reflect wave propagation in a 2D medium. It is a common practice to apply the standard 3D to 2D correction Crase et al. (1990)

- data multiplication with $\sqrt{t}$
- convolution with $1/\sqrt{t}$

It should be noticed that this correction is valid only for 1D media but fails in the presence of lateral heterogeneities in the model.

SOURCE PROPERTIES

Wavelet estimation

An accurate description of the source signature and realistic modeling of the source ghost effect are necessary for successful inversion. The source wavelet was estimated from direct arrivals to a hydrophone

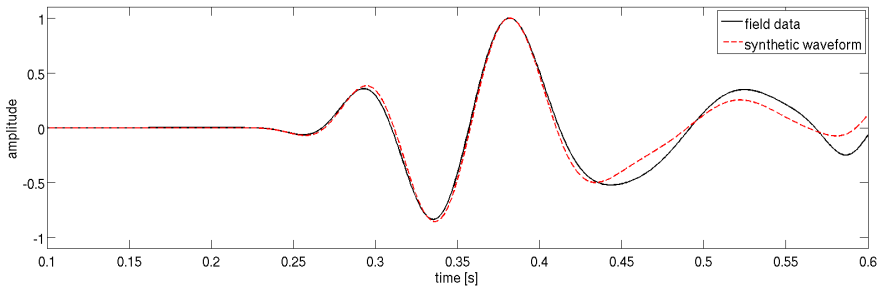

Figure 5: Comparison of the synthetic direct arrival modeled with the estimated wavelet in Figure 4f, with the field direct arrival waveform. A bandpass filter was applied.

group Kravis (1985). The response of a hydrophone group to a pressure impulse transmitted from a source consists of two impulses: 1) ray traveling directly from the source to the hydrophone, 2) source ghost reflection from the air/sea interface. When the upward-traveling initial signal reaches the sea/air interface it is reflected with an opposite polarity and becomes a ghost. Mainly because of the large difference in density between air and water, the sea/air interface acts like a mirror to pressure waves traveling from the source.

The source signature estimation is based on the hydrophone response deconvolution from the observed direct arrivals. This method requires that there is no interference between the recorded direct arrivals and the seabed reflections or refractions. The response to an impulse traveling horizontally from the source is computed for a single hydrophone, based on the modeling parameters. Therefore, the estimated wavelet is an optimum wavelet designed for specific FD parameters. The reciprocal of the horizontal impulse response represents the inverse operator. Afterwards, this inverse impulse is convolved with the recorded direct arrivals by a frequency domain multiplication. The result of this convolution provides an estimate of the source signal, Figure 4.

Airgun array simulation

airgun	average Volume C.I.	$A \propto V^{1/3}$	normalized amplitude
1	500	7.94	1
2	268	6.45	0.81
3	140	5.19	0.65
4	72	4.16	0.52
5	42	3.48	0.44
6	179	5.64	0.71

Table 1: 2D airgun array layout, based on the true 3D array characteristics (Figure 6)

In this seismic experiment the airgun array with 24 individual airguns and a total volume of 4804 inch^3 was used as a seismic source. In contrast to a single airgun, an airgun array shows strong directivity effects, especially at higher frequencies. Moreover, each array has its own specific radiation pattern, i.e. the source signature changes as a function of direction (horizontal angle) and emission angle. To investigate whether the single point source approximation of an airgun array is accurate for waveform inversion, we analyze the

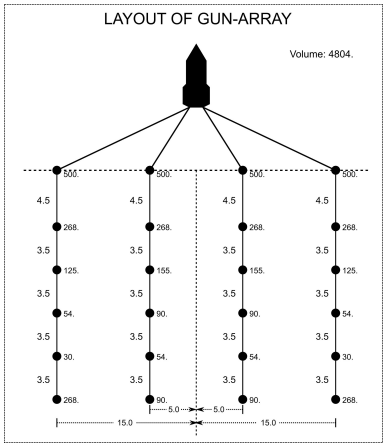

Figure 6: Field airgun array configuration.

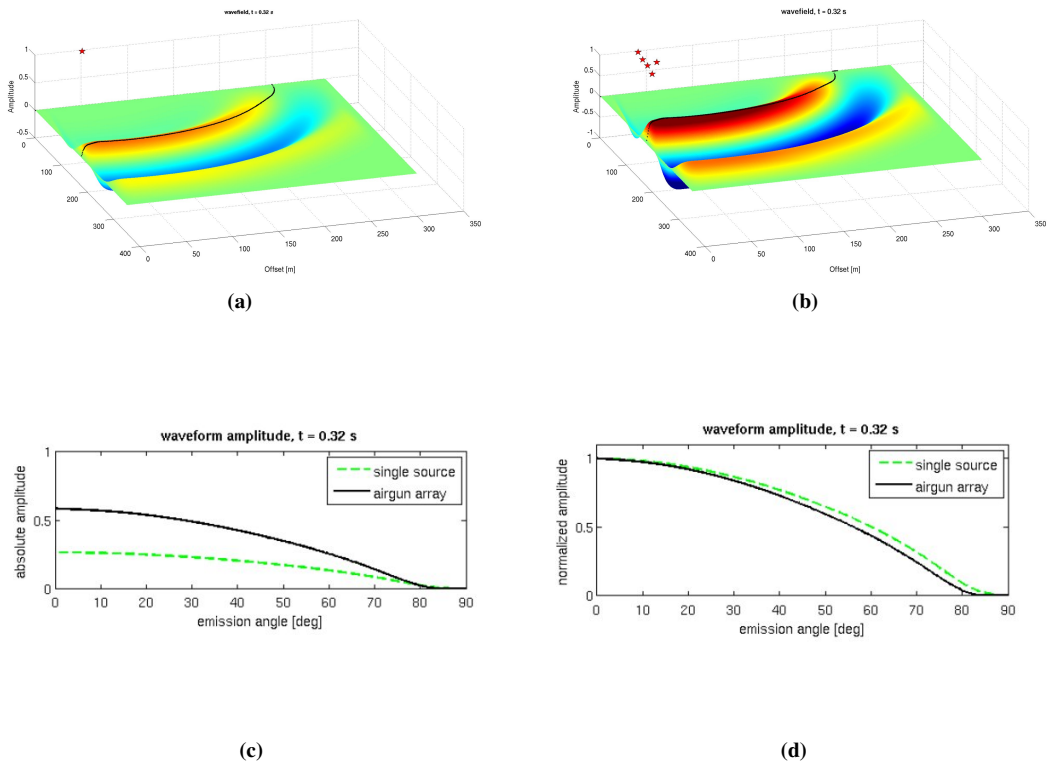

Figure 7: (a) Radiation pattern of the single airgun, and (b) the airgun array (Table 1) in the water column. Comparison of the absolute (c) and normalized (d) wavefront amplitudes (solid lines at Fig. 2a and 2b) as a function of the emission angle. The wavefield was generated using a band limited signal (3-20 Hz), i.e.the estimated wavelet filtered with Butterworth filter 3-14 Hz.

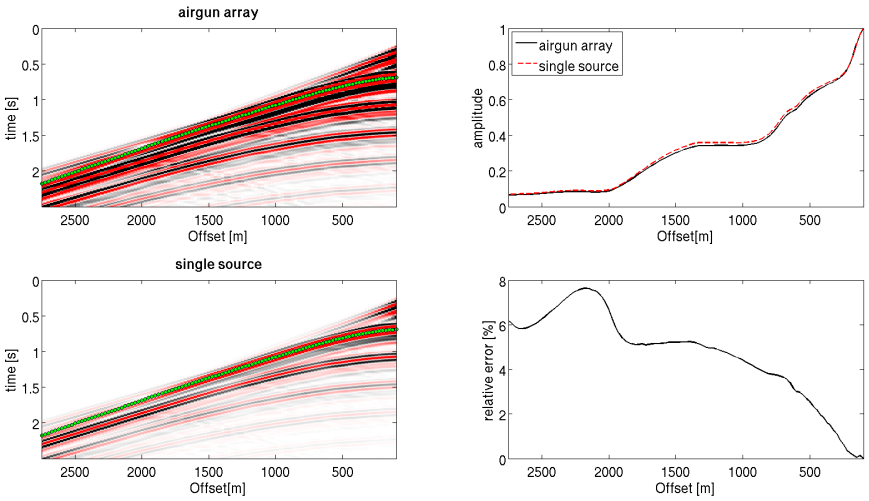

Figure 8: Waveform generated by the airgun array (top left) and the single airgun (bottom left); the field acquisition settings and the starting model (Figure 9) were used. Right: comparison of the primary reflection amplitudes (green dots on the seismograms) for the both shot gathers; top: normalized amplitude, bottom: relative error. The main discrepancy occurs at offsets smaller than 1500 m. Because of the directivity effect, the single source approximation is not sufficient for a realistic description of the amplitude behavior of the recorded data.

radiation pattern of the source array (Table 1) and the point source. The maximum frequency of the source signal used in these tests is 20 Hz, that corresponds to the highest frequency content of the field data used in the inversion. When comparing the radiation images in the water column in Figure 8, it can be seen, that most of the energy emitted from the airgun array is concentrated close to the vertical emission angle, and the pressure amplitudes in the horizontal direction are smaller than that from the point source. The amplitude rapidly diminishes at emission angles greater than 80°. The difference in the directivity effects is also measured for the amplitude versus offset behavior of the seafloor reflections, generated with these two source types (Figure 8). For the frequency range used in the simulation (up to 20 Hz) the relative error of the point source is less than 10 %, and the difference in directivity effects of an airgun array and a point source increases with offset. In spite of this relatively small difference, all inversion tests employ an airgun array, so that the modeled waveforms accurately reproduce the directivity effects of a source array.

STARTING MODEL

Marine seismic data are always band limited and lack low frequencies. Therefore a good starting model is necessary to fill in the gap of low frequencies before the inversion of available frequencies. Using a poor starting model would cause slow convergence, large misfits, or unrealistic results in this case. Due to the lack of frequencies below 3 Hz in our field data, the background velocity model cannot be precisely recovered by the FWT. Therefore it is necessary to construct an initial velocity model that already contains the long wavelength features of the subsurface.

The starting velocity model (Figure 9b) for the waveform tomography is based on the interval velocities calculated from the vertical seismic profiling (VSP) data available from the borehole located in the middle of the selected region. The original interval velocity model was smoothed, so that the individual layers are replaced by a gradient. Velocity ranges from 1480 m/s in the water layer up to around 3200 m/s. In addition, the density information is also required in numerical modeling of marine environment, mainly to simulate an accurate amplitude of the seabed reflection and multiples. The density model is computed from the velocity model based on Gardner's velocity-density relationship (Gardner et al., 1974). To account for multiple reflections and the ghost effects present in the data, the air layer was implemented at the top of the model. The velocity and density models are discretized on a mesh with 656 $\times$ 660 grid points, using 5 m

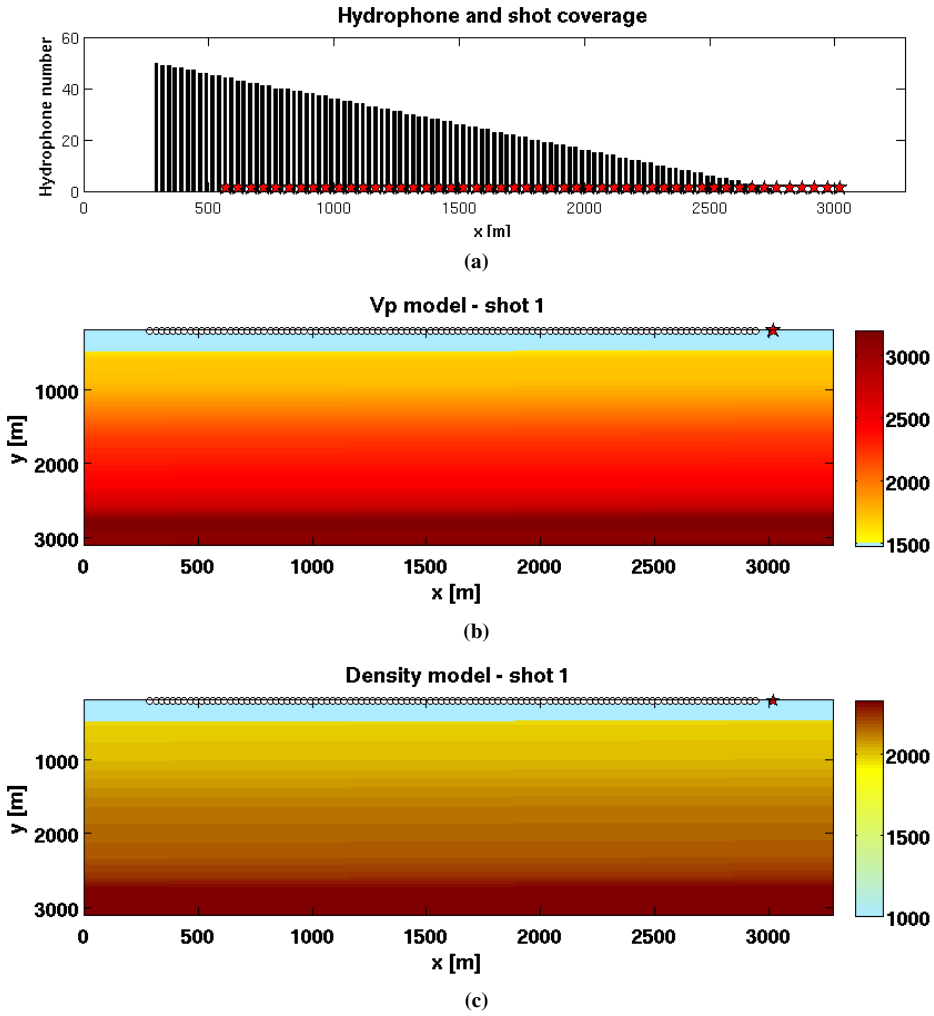

Figure 9: (a) Acquisition setup that is used in the field data inversion. Starting P-wave velocity [m/s] (b) and density (c) models [kg/m^3]. The acquisition layout shown in Figures (b) and (c) are used to generate synthetic data in the initial forward modeling. The circles indicate the locations of 107 hydrophones, the array source is used.

grid spacing.

INITIAL MODELING AND AMPLITUDE SCALING

Prior to the waveform inversion the initial forward modeling is performed. It is an important step to evaluate the starting model and to evaluate whether the waveform inversion is likely to succeed. If the observed waveform is not matched to within a half-cycle by the synthetic data generated from the starting model, it is likely that the algorithm will attempt to fit the calculated events to the wrong cycle of the observed data, and the solution may start to diverge. The results of the initial modeling are also used to scale the synthetic and observed data.

To compensate for the unknown source strength, the sensitivity of the recording system, and scaling factors within the finite difference modeling code, amplitudes of the field shot gathers must be scaled with the corresponding amplitudes of the initial synthetics. This can be achieved by scaling the amplitudes of the seabed reflection event at the nearest offset. To use this approach, the starting model must already contain an accurate information of the true seafloor parameters, because the seafloor reflection in each field gather is equalized to the value of the synthetic data. The AVO (amplitude versus offset) analysis performed for different field shot gathers (Figure 10) shows a significant difference in the amplitude decay with offset. These amplitude variations indicates the change of material parameters of the seafloor sediments along the profile. Moreover the match between the field and synthetic seafloor reflection amplitudes is not good enough to exclude the seafloor region from the inversion.

Amplitude calibration can be also performed by balancing the amplitudes around the direct arrival at the nearest offset channel. This approach requires a close fit of the modeled direct arrival to the one observed in the field data. Therefore, a proper description of the acquisition parameters, a good estimate of the source signature, and an accurate modeling of the directivity effects is necessary. However, this method allows the update in the seafloor region and it normalizes variations in the source strength between the shots.

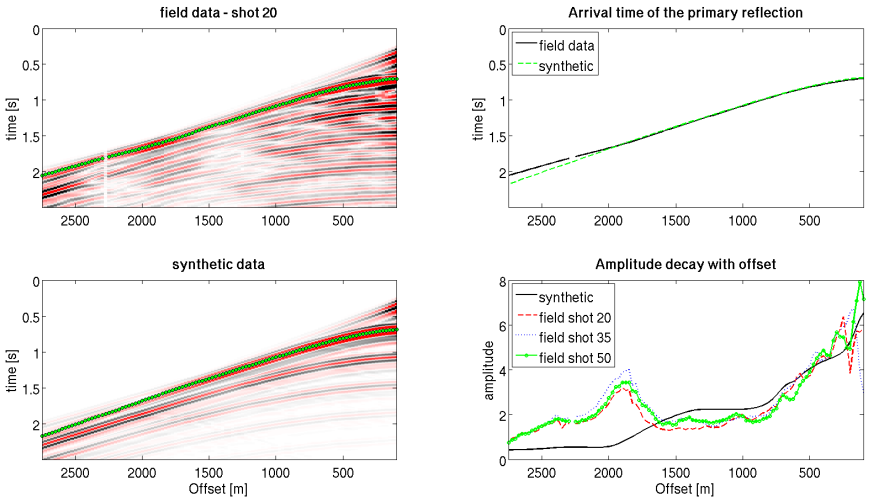

Figure 10: (top left) Field data after preprocessing: shot 50, the maximum amplitude values (green dots) picked from the field data correspond to the seafloor reflection for offsets up to 1600 m, and to the refracted wave for offsets greater than 1600m. (bottom-left) FD modeled initial synthetics, green dots indicates the seafloor reflection. The direct comparison of the amplitude-versus-offset behavior of the seafloor reflection between the simulated and field data is only possible for offsets smaller than 1600 m. (top right) The arrival time of the reflected wave is matched well by its synthetic counterpart. This will help to avoid cycle-skipping artifacts during the waveform inversion. (bottom right) The amplitude-versus-offset behavior of the seafloor reflection from the synthetic data and three field shot gathers. The sharp amplitude variations visible at the near offset traces are probably due to the inaccuracies of the 3D to 2D transformation in the near field. These traces are precluded from inversion.

RESOLUTION TEST

To test the resolving power and the reliability of FWT results we constructed a synthetic model and calculated acoustic data using the same acquisition geometry, source signature and data sampling as in the field example. Results from the synthetic inversion will help us to identify artifacts due to the source-receiver geometry limitations (ray coverage), or choice of a poor starting model, and will allow to determine which parts of the model can be well resolved. They are also useful for designing inversion strategies that are suitable for the analyzed field data.

A true velocity model was generated by adding $\pm$ 5 % velocity perturbation to the initial velocity model for FWT. The checkerboard anomaly size of 150 m corresponds with the average wavelength generated by the narrow band source. The streamer geometry comprised 50 shots with a shot spacing of 50 m and total of 2540 receivers with a spacing of 25 m. The final inverted model ((Figure 11e) is an excellent recovery of the true model up to the depth of 1700 m, which is also reflected in the final residuals. Artifacts that are visible at the edges of the model and at greater depths result from an insufficient ray coverage in these areas. To improve the subsurface coverage and to resolve deeper structures it will be necessary to increase the hydrophone number and to include later arrivals.

DENSITY EFFECT

In this experiment we want to investigate the effect of density information on the recovery of P-wave velocity models in the marine environment. The true density model is calculated from the velocity model (Figure 12) using the Brocher's density-velocity relationship, (Brocher, 2005):

$$\rho(g/cm^3) = 1.6612V_p - 0.4721V_p^2 + 0.0671V_p^3 - 0.0043V_p^4 + 0.000106V_p^5 \quad (1)$$

The perfect starting initial V_p model is used in the inversion, so that we can explicitly illustrate the waveform tomography dependence on the choice of a density model. The source wavelet and acquisition geometry used in these tests are the same as in the field data example. We have tested four different strategies of including the density information to the inversion scheme:

- TEST 1 - homogeneous density model; no density update; (Figure 13)
- TEST 2 - density is linked with the starting P-wave velocity model using Gardner's relationship; no density update; (Figure 14)
- TEST 3 - density is linked with the inverted P-wave velocity model using Gardner's relationship; density is updated after each iteration step ; (Figure 15)
- TEST 4 - separate density and velocity inversion; (Figure 16)

As the the reflection coefficient at the seafloor is primarily governed by a high density contrast it is necessary to include the density information in the waveform tomography. Excluding the density parameter from modeling and inversion results in incorrect modeling of the seafloor reflection and multiple amplitudes and produces strong artifacts around the seafloor (Figure 13). Poor recovery of the velocity model is also reflected in high amplitudes of the residual waveform.

In tests 2-4 we used Gardner's relationship for estimating density from P-wave velocity. The relation takes the following form:

$$\rho(kg/m^3) = 0.31 * 1000 * V_p^{0.25} \quad (2)$$

Gardners's rule seems to be the standard in the exploration geophysics. This relation is simply an approximate average of the relations for a number of sedimentary rock types, weighted toward shales. It should be noticed that the true velocity-density relationship is different to that assumed in the inversion scheme.

The final inversion results from TEST 2 (Figure 14) and TEST 3 (Figure 15) show significant improvement in the imaging of upper parts of the P-wave model if the density model is included. However, for this particular case, keeping the density model fixed during the inversion or updating it from the velocity model after each iteration have no effect on the final velocity model.

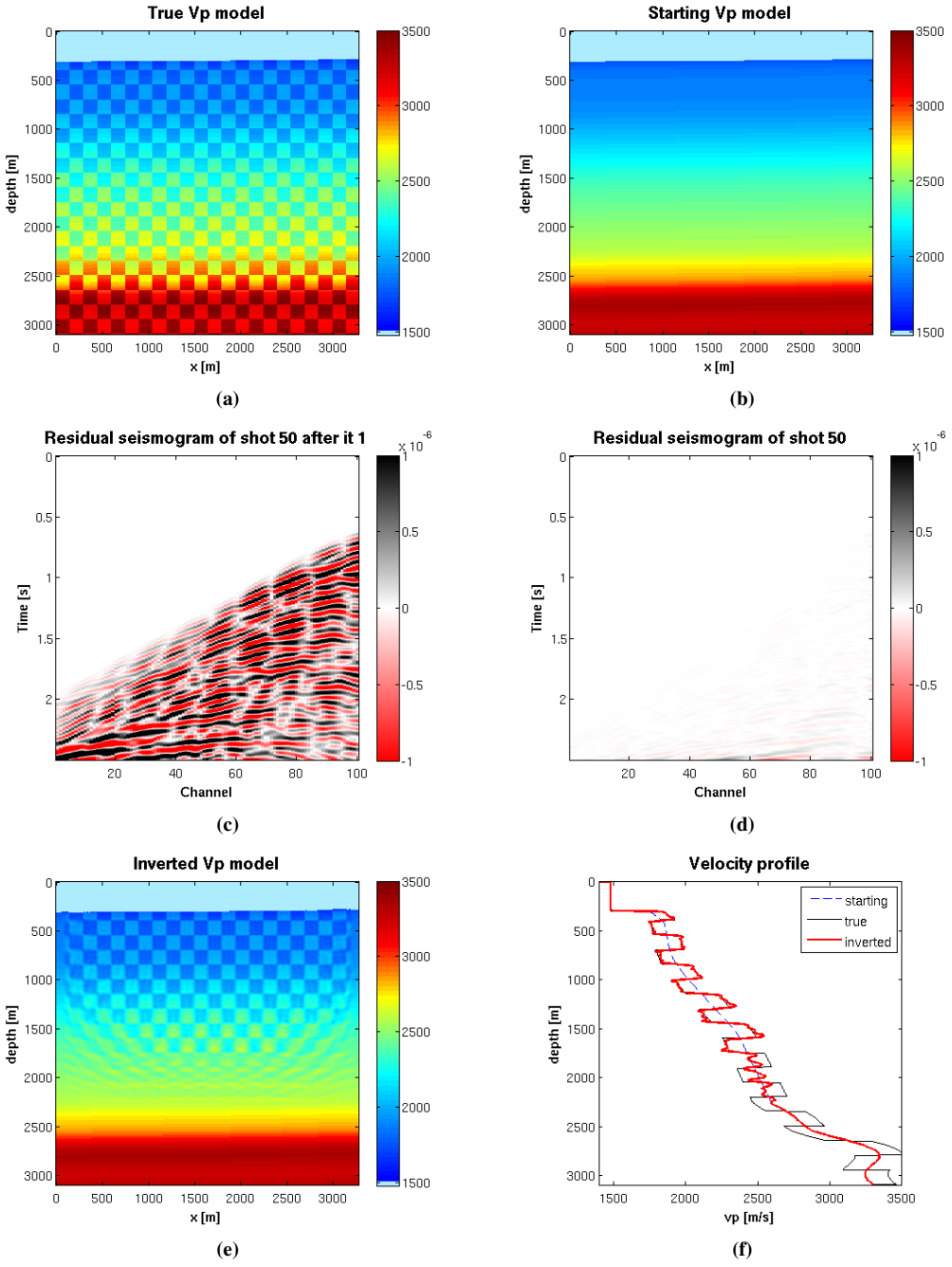

Figure 11: FWT results for the resolution test after 500 iterations. (a) True V_p model [m/s], (b) starting model for the inversion, (c) initial residuals, (d) final residuals, (e) inverted V_p model after 500 iterations, (f) velocity profiles.

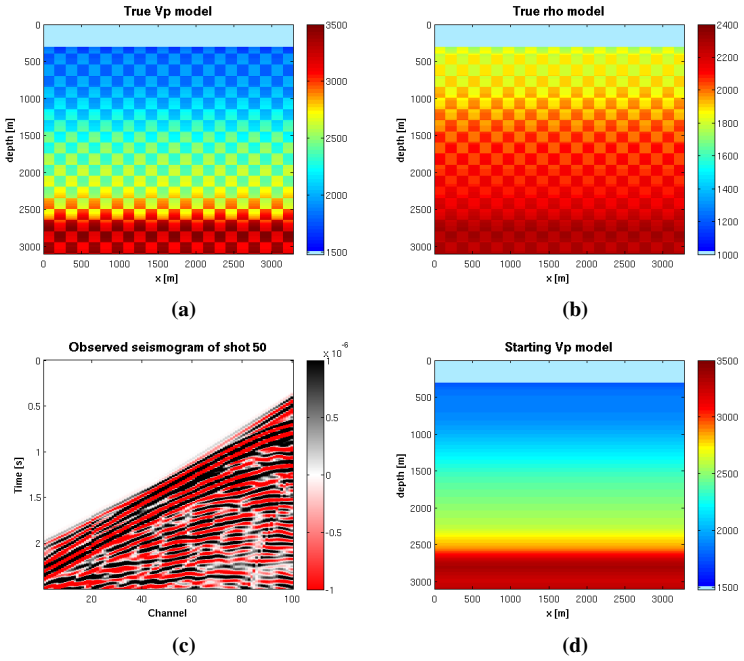

Figure 12: (a) True velocity [m/s] and (b) density models [kg/m^3], (c) modeled seismograms for shot 50, (d) starting V_p model for the inversion.

Figure 16 shows the waveform tomography results for the separate, alternate density and velocity inversion. Simultaneous inversion for both of these parameters produced strong imaging errors, therefore only one parameter is updated at each iteration step. The final inversion result shows that there is no major improvement in the P-wave velocity model, and only the artifacts around the seafloor are slightly reduced.

Estimating density values from seismic data is an ill-posed inverse problem. Inversion for a density is usually unstable even for moderately noisy data and requires additional constraints to stabilize the inversion. Tarantola (1986b) found that the misfit function of marine data is most sensitive to updates of the seismic velocities, and the effects from density model updates are much smaller. This implies that the inversion scheme is least sensitive to errors in density and even a poor starting model for density has no significant influence on the quality of the velocity models.

INVERSION STRATEGIES—ROLE OF THE PRECONDITIONING

The aim of full waveform tomography is to find a model which explains the observed data, i. e. it minimizes the data misfit function between observed and modeled data. The misfit or data residuals δu are measured by the L2-norm, and an optimum model can be found in the minimum of the residual energy. Therefore the following objective function has to be minimized:

$$E = |L_2| = \frac{1}{2}\delta u^T \delta u \rightarrow \min \tag{3}$$

To find an optimum model the material parameters (velocity, density) are updated iteratively along the conjugate gradient direction δc with the step length μ_n:

$$m_{n+1} = m_n - P\mu_n \delta c_n \tag{4}$$

where m_{n+1} is the model update at iteration i+1, and P the preconditioning operator.

In some cases the high complexity of the seismic data or high noise level might cause a very complex and nonlinear data misfit function, and it might generate unrealistic model parameter updates. To control the model update and to improve the convergence and/or the linearity of the inverse problem different preconditioning methods can be used. Basically the full waveform tomography algorithm can be implemented

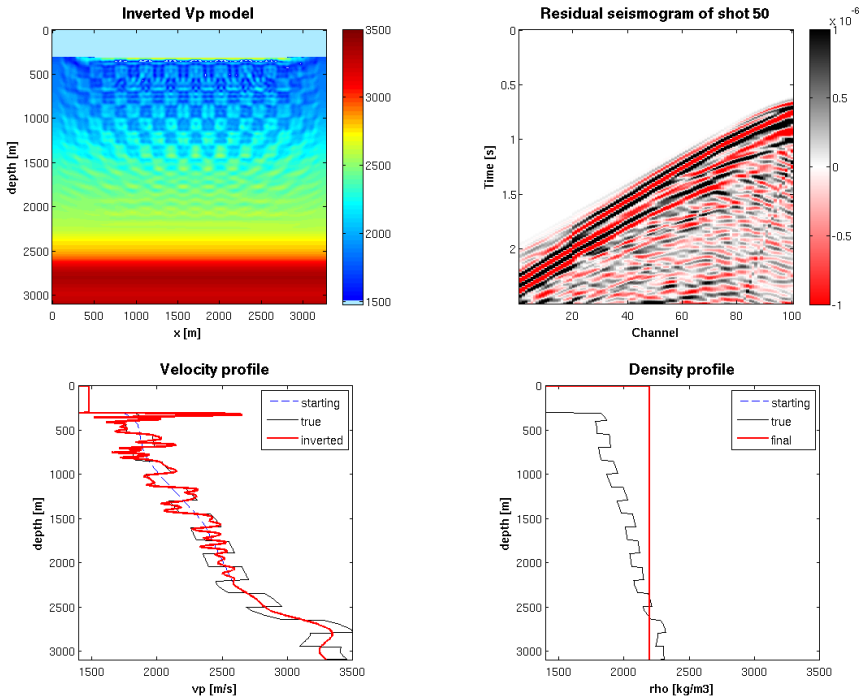

Figure 13: TEST 1: FWT results after 500 iterations for the homogeneous density model.

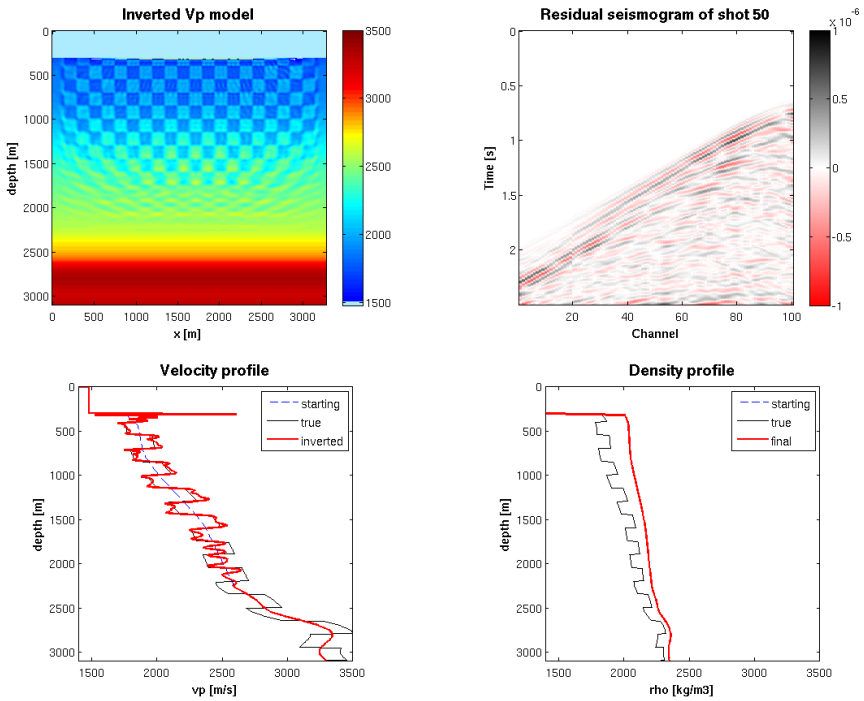

Figure 14: TEST 2: FWT results after 500 iterations for the fixed density model, computed from the starting V_p model using Gardner's relationship.

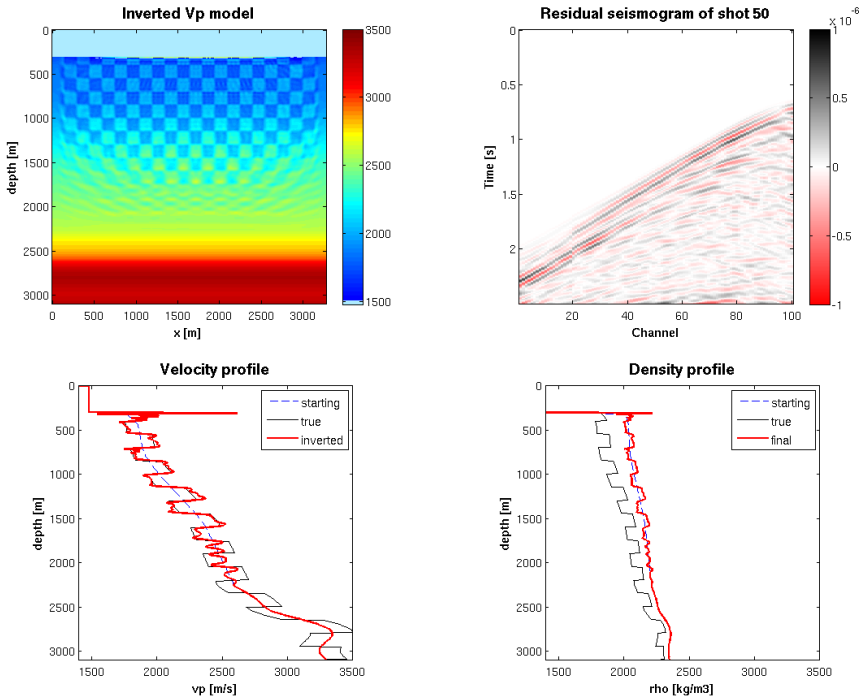

Figure 15: TEST 3: FWT results after 500 iterations. The density model is updated after each iteration step from the current V_p model using Gardner's relationship.

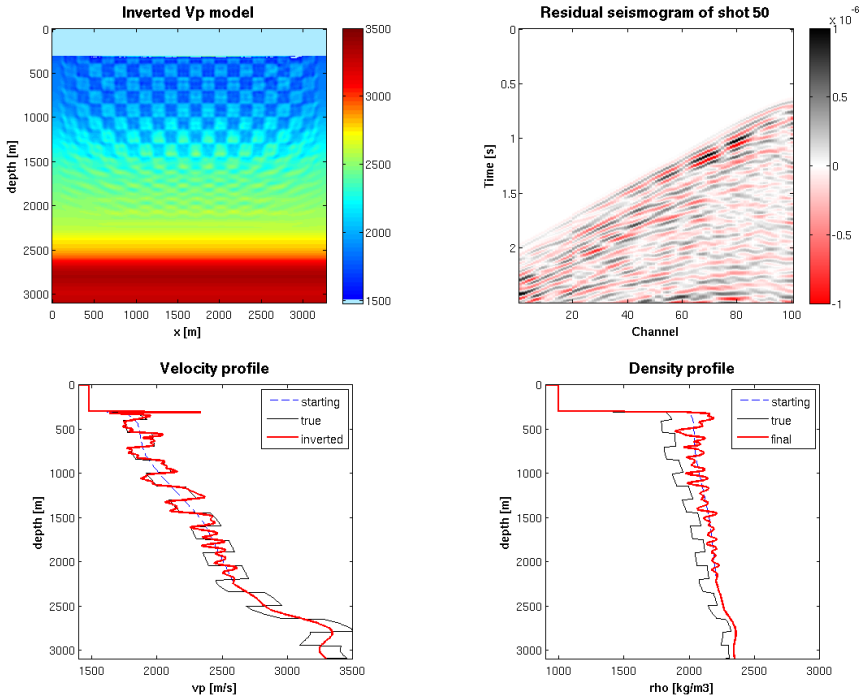

Figure 16: TEST 4: FWT results after 500 iterations for the separate density and velocity inversion.

in the time or in the frequency domain, and the choice of a domain constraint the preconditioning methods that can be applied to the data or to the gradient. A regularization scheme in the time domain can be realized by applying time windowing and frequency filtering to the data, or by applying a preconditioning operator that modifies the gradient.

The calculation of the velocity gradient resulting from the waveform cross-correlation is a crucial part in the waveform tomography. This quantity describes how to optimize the starting model or the model from the previous iteration step. The preconditioning operator P that can be applied to the gradient approximates the inverse Hessian matrix. There is no general rule to design this parameter:

$$P = H_1^{-1} = \left(\frac{\delta^2 E}{\delta m^2} \right)^{-1} \tag{5}$$

To demonstrate the effect of the preconditioning, we performed various synthetic inversion tests using the checkerboard model. Synthetic data are calculated using the same P-wave velocity model and acquisition setup as in the previous section. The source signature is the wavelet estimated from the field data which covers a frequency bandwidth of 3-20 Hz. The starting model for FWT has been modified, so that the background velocities of the true model are shifted by 6 %.

No preconditioning

For the first inversion test no preconditioning methods were applied. Figure 17 shows the inverted V_p model after 500 iterations. The velocity structures of the true model are only well recovered in the upper part of the model, but resolution and accuracy decrease very quickly with depth. Moreover, a lot of artifacts are present in the inverted model. This final result is not as close to the true model as the result obtained in the resolution test (Figure 11), where inversion was able to correctly image structures up to 1700m. However, it should be noticed that an unrealistically accurate starting model is used in the resolution test. Therefore the nonlinearity of the inversion problem is significantly reduced at the same time. This inversion example clearly shows that the lack of low frequencies in the data combined with the use of a starting model, that does not contain the long-scale features of the true model results in a quite poor recovery of a velocity model.

Preconditioning operator

The inverted model from the previous example shows strong artifacts close to the air/water interface, near sources and receivers, and in the water column. To suppress these large gradient values, a spatial preconditioning operator is applied to the gradient. It sets the gradient in the water layer to zero, i. e. it turns off the velocity update in this part of the model. To eliminate these artifacts, an optimum preconditioning operator has to be designed for a specific acquisition geometry and starting model, i. e. the depth to the seafloor must be known. To improve the stability of the inversion, especially in a real data case, the gradient smoothing operator can be applied. Such a 2D spatial filter removes high frequency artifacts from the gradient.

Furthermore the linear gradient scaling with depth is implemented. It is supposed to correct for the amplitude loss with depth due to the geometrical spreading and to enhance deeper parts of the model. Otherwise, the early arrivals would dominate the data fitting in the inversion scheme, and velocity updates in the upper parts of the model would be more significant than in the deeper parts. After application of the preconditioning operator, all strong artifacts within the water layer are removed, and there is an improvement in the recovery of deeper structures (Figure 18).

Time windowing and frequency filtering

By the application of time windowing during the inversion process, the amount of information is gradually increased with the increasing propagation time of seismic waves. The reduction of data by time windowing allows the algorithm to update the upper part of the model in the first instance and then proceed to deeper parts of the model. If a poor starting model is used, time windowing would help to decrease the nonlinearity caused by the inaccurate initial model parameters. However, the time window should be designed carefully, otherwise it might produce some artifacts and decrease the resolution of the deeper model parts.

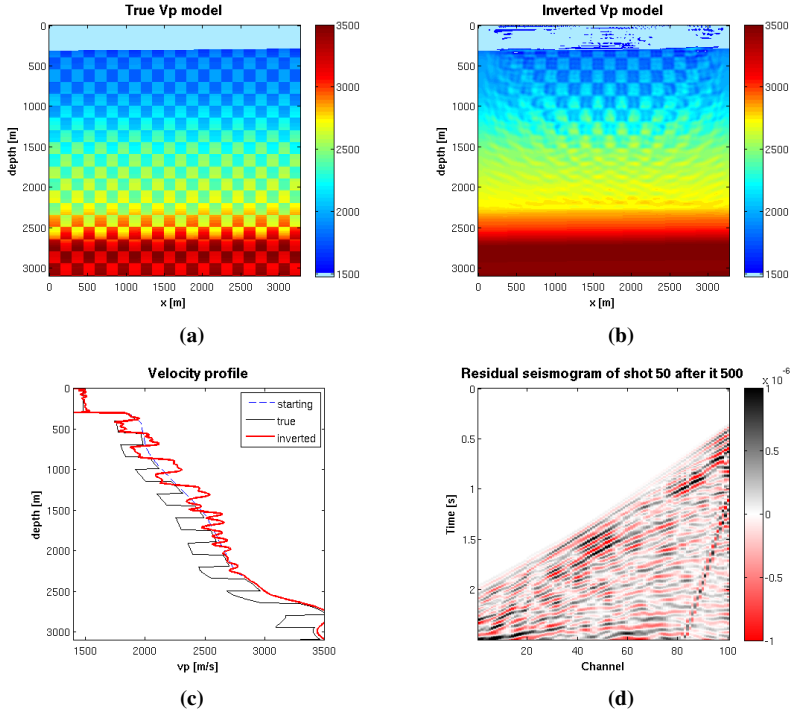

Figure 17: FWT results after 500 iterations, no preconditioning applied. (a) True V_p model [m/s], (b) the inverted V_p model [m/s], (c) velocity profiles, (e) final residuals.

In the previous examples the full data information was used in each iteration step. Figure 19 demonstrates the results with the application of time windowing and gradient preconditioning techniques described in the previous tests. An initial window of 1 s is increased linearly from the iteration 50 until it covers the full record length of 2.5 s. We can observe an additional improvement in the reconstruction of the velocity model after application of time windowing. The final inverted model is much closer to the true model than the inversion result for an exclusive application of gradient preconditioning.

The nonlinearity of the objective function is frequency dependent, i. e. the shape of the objective function depends on the frequency content of the seismic data. At lower frequencies the objective function is smooth, while a lot of local minima are present at higher frequencies. Therefore, the inversion should start at the lowest possible frequencies and add higher frequency content gradually.

Another inversion run was performed to illustrate the effect of the combined application of frequency filtering and time windowing. In this case, the multistage inversion approach is used. In stage 1, only data containing frequencies of 3-7 Hz are inverted, in stage 2 of 3-15 Hz, and in stage 3 of 3-20 Hz. The result from each lower frequency inversion is used as the starting model for the next higher frequency inversion. At each frequency stage, 300 iterations are carried out. For each iteration scaling with depth, mute within the water layer, and spatial filter is applied to the gradient. Figure 20 shows the final reconstructed image after all three stages, along with the intermediate results. The very good fit between the final and the true model can be also observed in the final residuals.

Comparing the final result of the multi-stage (Figure 20) and the single-stage (Figure 19) inversion, we can see that the combination of frequency filtering with time windowing provides a comparable reconstruction of the velocity model as the inversion with the exclusive application of time windowing. In this experiment the starting model is evidently accurate enough, so that the application of time windowing and gradient preconditioning is sufficient to reconstruct a high-resolution velocity image. However, if a poor starting model and noisy data are used, the multi-stage inversion would be an optimum choice to improve both the convergence and the inversion results.

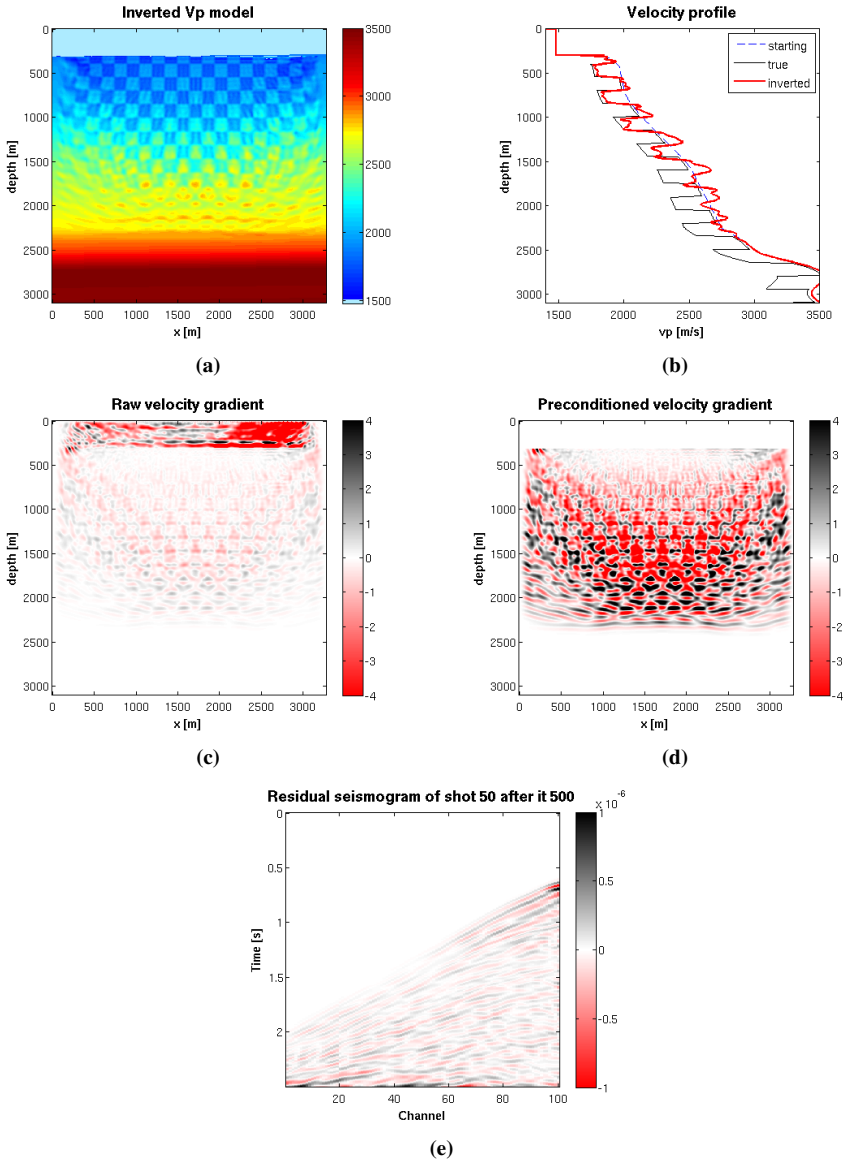

Figure 18: FWT results after 500 iterations; velocity gradient scaling with depth and gradient taper within the water layer are applied.(a) The inverted V_p model [m/s], (b) velocity profiles, (c) raw V_p gradient, (d) preconditioned V_p gradient, (e) final residuals.

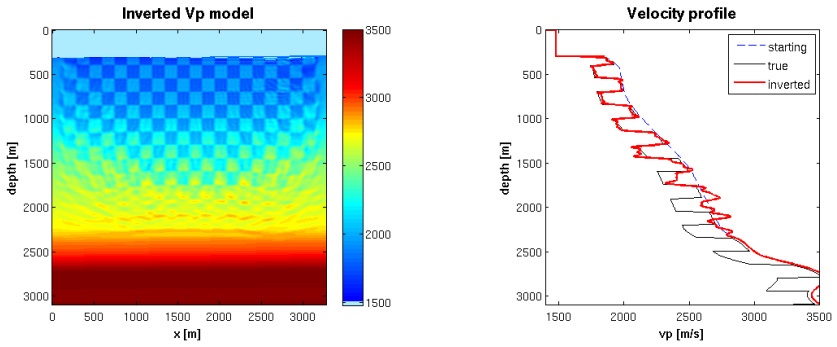

(a) (b)

Figure 19: FWT results after 500 iterations; time windowing and velocity gradient preconditioning are applied. (a) The inverted V_p model [m/s], (b) velocity profiles.

FIELD DATA INVERSION - PRELIMINARY RESULTS

Full waveform inversion of the field data is performed using 50 shot gathers with a variable number of hydrophones (Figure 9a). This geometry assures the highest ray coverage for a given model size. The near offset is 255 m with a receiver increment of 25 m. Checkerboard resolution test indicates, that for this acquisition setup and a recording length of 2.5 s, a velocity model can be well resolved down to about 1.7 km below the water surface.

Two inversion tests are carried out for different frequency content. In the first test only the low frequencies are inverted. The estimated wavelet and preprocessed field data are band pass filtered and contain frequencies between 3.5 and 7 Hz. In the second test a higher frequency content is included; 3-15 Hz. The same starting V_p and density models (Figure 9) serve as an input for both inversion experiments. In order to reduce the complexity of the inversion problem various preconditioning techniques are exploited: velocity gradient tapering within the water layer, linear gradient scaling with depth, gradient smoothing and time windowing. Moreover, some absolute and relative model restrictions have been applied to the model update, in order to avoid unrealistic velocity and density values. To stabilize the inversion, the maximum deviation of the velocity model from the model of the previous iteration cannot exceed 1%.

The inverted velocity models after 500 iterations are shown in Figure 21, for the frequency content 3.5-7 Hz in the left part of the figure, for the frequency content 3-15 Hz in the right part. Although the overall misfit of the data has decreased, there are a lot of strong artifacts present in the reconstructed velocity images, especially including areas with unrealistic low velocities. Since there are no structures that would be common for both inverted models, we have to assume that the recovered models predominantly consist of inversion artifacts.

Synthetic tests show that the quality of the FWT results improves significantly, if the data is inverted separately for different frequency content, starting at low frequencies and adding higher frequency content gradually. However, as there is a significant level of low-frequency swell noise in the field data, starting the inversion at low frequencies has produced unrealistic results. Therefore, it would be necessary to investigate the effect of coherent and non-coherent noise on the waveform inversion performance and to attenuate noise in the field data. Some of the imaging errors are also due to the insufficient estimation of the source properties. Therefore, a more accurate description of the source wavelet would be a necessary condition for successful waveform tomography. An individual signature should be computed for each shot by means of source wavelet inversion.

The comparison between the observed and inverted waveform shows a reasonably good match (Figure 22), while the corresponding velocity models contain a lot of unrealistic structures. As mentioned before, the aim of waveform inversion is to derive a velocity model that produces the best fit to the seismic data, i. e. to the phase and to the amplitude content. The L2 misfit function does not separate phase and amplitude information, but it minimizes the residuals of the pressure amplitude. As the density model is updated using the velocity-density relationship at each iteration, inversion of amplitudes and phases means

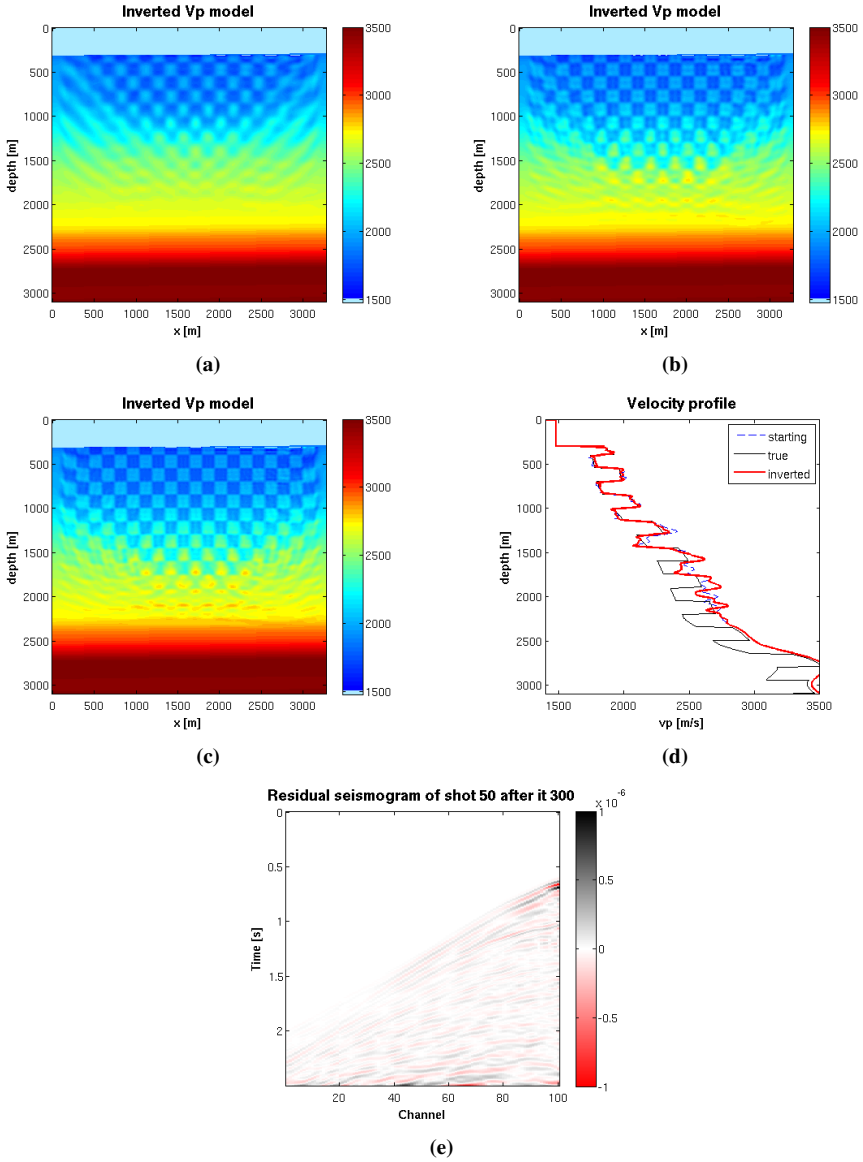

Figure 20: FWT results for the multi-stage inversion. (a) The inverted V_p model [m/s] after stage 1 (3-7 Hz), (b) the inverted V_p model [m/s] after stage 2 (3-15 Hz), (c) the inverted V_p model [m/s] after stage 3 (3-20 Hz), (d) velocity profiles, (e) final residuals.

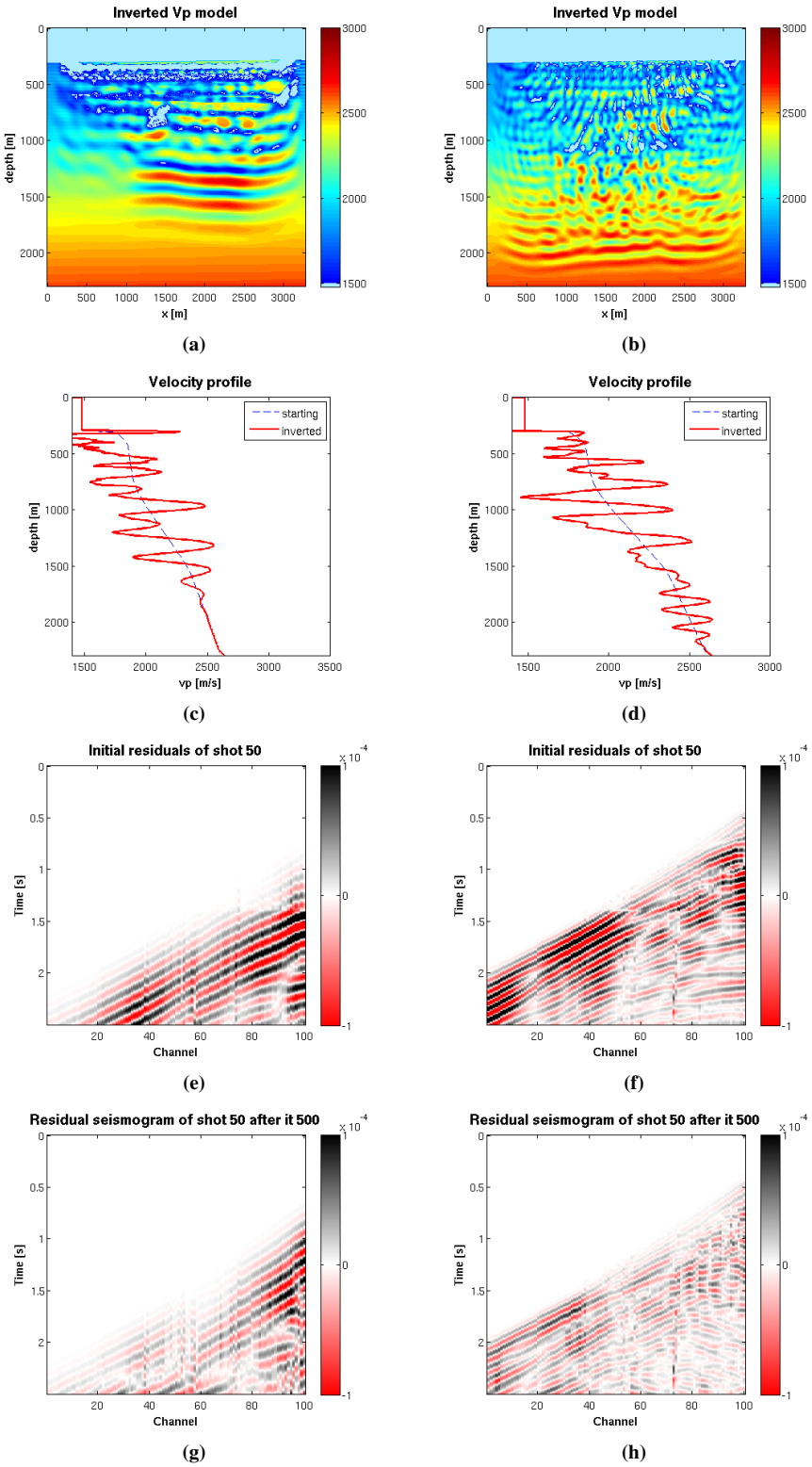

Figure 21: FWT results for the field data inversion, left: frequency content 3.5-7 Hz, right: frequency content 3-15 Hz; (a),(b) The inverted V_p model [m/s]after 500 iterations; (c),(d) velocity profiles; (e),(f) initial residuals for shot 50; (g),(h) final residuals for shot 50.

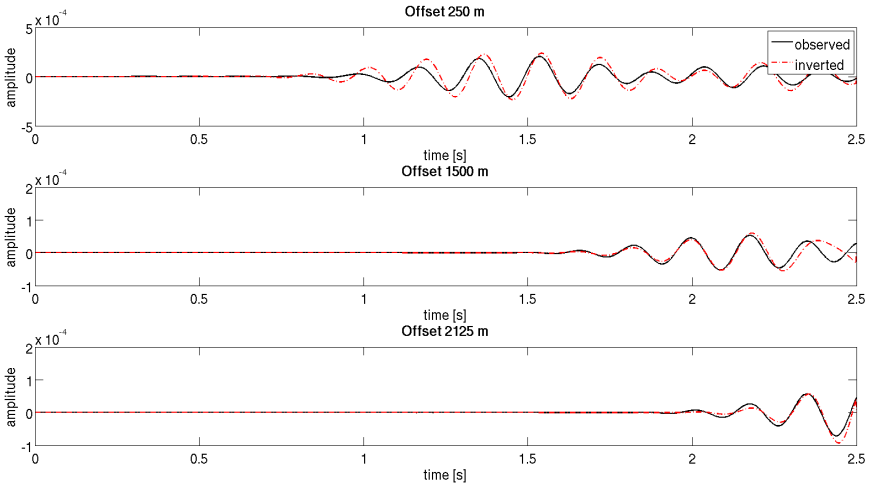

(a)

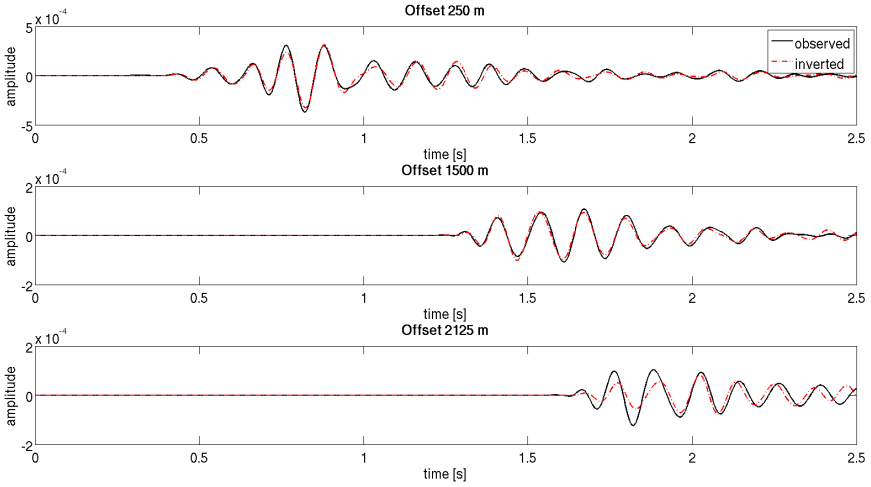

(b)

Figure 22: The comparison between the observed and inverted waveform for different offsets. (a) 3.5-7 Hz, (b) 3-15 Hz.

projecting these variations onto velocity perturbation. This may produce unrealistic velocity values, because most of the information about the P-wave velocity is contained in the phases, whereas amplitudes are also sensitive to density information, attenuation, and to converted waves. Since the phase and the amplitude information cannot be separated in the time-domain approach to perform phase inversion only, it might be necessary to normalize the field data amplitudes and include the density inversion.

Moreover, inversion based on the acoustic wave equation does not take the S-velocity into account, therefore the various seismic events such as ground roll, multiples, mode conversions and S-wave events are treated as undesirable coherent noise. To correctly handle the multiples in the inversion scheme, the forward modeling should provide the accurate amplitude and arrival times of the multiples. Since the seabed reflections and multiples have high amplitudes, any mismatch between the real and modeled events will result in strong artifacts. Sea surface waves variability, which cannot be modeled by the FD code, elastic effects (i. e. amplitude versus offset behavior) and lack of attenuation information in the seafloor region will lead to inaccuracies in the modelling, and in the consequence will cause the divergence of the inversion algorithm. Therefore, we should attenuate multiples, remove the ghost effects generated at the air/water interface, and replace the free surface condition at the top of the model with an absorbing boundary. This should reduce the ambiguity of the inversion problem and improve the recovery of true velocity structures.

CONCLUSIONS AND OUTLOOK

In this paper we have discussed several practical issues in the application of the waveform tomography to the field data. We have demonstrated that the efficiency of FWT depends not only on the choice of the starting model, but also on methods which reduce the complexity of the inversion problem. The application of different preconditioning strategies such as time windowing, frequency filtering, gradient preconditioning and including the density information may lead to significant improvements in the subsurface reconstruction. The resolution analysis using the experimental setup provides the necessary guidelines to design a multi-scale inversion approach, which is suitable for the analyzed field data and reduces the nonlinearity of the problem. In conclusion, this improves the resolving power and the reliability of the inversion results.

Even though synthetic tests show the effectiveness of the FWT, the field data application is an extremely nonlinear problem. Elastic effects, attenuation, density information, as well as the unknown source signature and noise present in the data significantly reduce the convergence. Therefore, further work has to be undertaken in order to reconstruct realistic velocity models by means of the waveform inversion of the field data. Future studies will focus on:

- investigation of the seismic noise effect on FWT results and noise suppression to increase S/N ratio of the observed data;
- application of the Fourier-Bessel 3D to 2D transformation. This alternative approach, based on wavefield transform technique, will allow a more accurate quantitative comparison between 2D modeled and real 3D wavefields;
- multiple suppression in the field data to increase the convergence of the inversion algorithm;
- separate wavelet inversion for each shot gather as a part of the waveform inversion procedure. This will improve the match between the wavelet used for synthetic modelings and the real wavelet in the seismic data;
- analysis of the potential of amplitude normalization. This should reduce the nonlinearity of the objective function and suppress artifacts in reconstructed velocity images;

ACKNOWLEDGMENTS

This work was kindly supported by Verbundnetz Gas AG (VNG), Leipzig, and the sponsors of the *Wave Inversion Technology (WIT) Consortium.*

REFERENCES

Bohlen, T. (2002). Parallel 3-D viscoelastic finite difference seismic modelling. *Computers @ Geosciences*, 28(8):887–899.

Brocher, T. M. (2005). Empirical relations between elastic wavespeeds and density in the Earth's crust. *Bull. Seism. Soc. Am.*, 95:2081–2092.

Crase, E., Pica, A., Noble, M., McDonald, J., and Tarantola, A. (1990). Robust elastic nonlinear waveform inversion: Application to real data. *Geophysics*, 55:527–538.

Elboth, T., Pettersson Reif, B., and Andreassen, Ø. (2009). Flow and swell noise in marine seismic data. *Geophysics*, 74(2):Q17–Q25.

Gardner, G., Gardner, L., and Gregory, A. (1974). Formation velocity and density—the diagnostic basics for stratigraphic traps. *Geophysics*, 39:770–780.

Kravis, S. P. (1985). Estimation of marine source signatures from direct arrivals to hydrophone groups. *Geophysical Prospecting*, 33:987–998.

Mora, P. (1987). Non-linear two-dimensional elastic inversion of multi-offset seismic data. *Geophysics*, 52:1211–1228.

Tarantola, A. (1986a). Inversion of seismic reflection data in the acoustic approximation. *Geophysics*, 49:1259–1266.

Tarantola, A. (1986b). A strategy for nonlinear elastic inversion of seismic reflection data. *Geophysics*, 51:1893–1903.